Defence Science Journal, Vol. 70, No. 2, March 2020, pp. 113-121, DOI : 10.14429/dsj.70.13053


# A Comparison of Circular and Slotted Synthetic Jets for Flow Control in a Twin Air-Intake

Krishnakumar Rajnath Yadav, Akshoy Ranjan Paul*, Nithin Hegde, and Anuj Jain

*Motilal Nehru National Institute of Technology Allahabad, Prayagraj - 211 004, India*
**E-mail: arpaul@mnnit.ac.in*

**ABSTRACT**

The performance of an aircraft engine depends on air flow quality at the engine face / the exit of the air-intake also known as aerodynamic inlet plane (AIP). A single-engine aircraft has complex Y-shaped twin air-intake which causes severe flow separation, distortion and flow non-uniformity at the AIP. The present study compares the efficacy of slotted synthetic jet and a row of four circular synthetic jets attached to inner faces of a twin air-intake to improve aerodynamic performance at the AIP. The results are obtained using computational fluid dynamics. The velocity and vorticity plots show that lateral spread of the circular jets is limited as compared to the slotted jet. The circular jets are found to be weak as compared to slotted jet to prevent separation of main flow occurring in the twin air-intake. The various aerodynamic performance parameters, such as static pressure recovery coefficient, total pressure loss coefficient, distortion coefficient and secondary flow uniformity are compared for both the cases, exhibiting marked improvement in all these parameters. The study demonstrates that the slotted synthetic jets is a better option for controlling flow in twin air-intake as compared to a row of circular synthetic jets.

**Keywords:** Twin air-intake; Flow control; Synthetic jet; Vorticity; Static pressure recovery; Distortion coefficient

## NOMENCLATURE

| | |
|---|---|
| $p_s$ | Average static pressure at any plane |
| $p_{si}$ | Average static pressure at the inlet |
| $U_{avi}$ | Mass-averaged velocity at the inlet (m/s) |
| $P_{Ti}$ | Mass-average total pressure at the inlet |
| $P_T$ | Mass-average total pressure at any plane |
| $n$ | Number of computed data points |
| $C_L$ | Centerline length of air-intake (mm) |
| $s$ | Local streamline position along centerline length (mm) |
| $C_{PR}$ | Static pressure recovery coefficient |
| $C_{TL}$ | Total pressure loss coefficient |
| $DC_{60}$ | Distortion coefficient |
| $S_{io}$ | Secondary flow non-uniformity |
| $V_{yz}$ | Secondary velocity |
| $Re$ | Reynolds number |

## 1. INTRODUCTION

Air-intake is a critical part of aircraft propulsion system, which ensures the required quantity of air supply to the engine for a wide range of speeds at different altitudes during flight. The latest generation single-engine combat aircrafts use Y-shaped twin air-intakes, the two inlets of which are mounted on either side of the fuselage and induce atmospheric air into the engine compressor. In order to meet the stealth requirement, the air-intake is made compact[1]. Due to the space constraint, the air-intake needs to be highly curved, which causes increased flow separation on the curved surface creating flow distortion and severe flow non-uniformity at the exit of air-intake / engine face commonly known as aerodynamic inlet plane (AIP). The flow distortion causes premature engine surge and flow non-uniformity may further cause a range of undesirable effects including asymmetric loading on the compressor blades. Therefore, employing the technique which controls the flow inside the air-intake and prevents flow separation may be significant in improving the overall efficiency, durability, and performance of the aircrafts[2].

Flow control techniques have been used for many years to control the fluid flow in many situations. Traditionally, flow separation management techniques are classified as active or passive, betting on whether or not management involves energy expenditure or not[3]. Vortex generator, surface roughness, trips, bumps, and dimples are some known examples of passive flow control techniques, where no additional energy is supplied from external source. Some researchers[4-6] employed different concepts of flow control in air-intakes in the last decade. However, one disadvantage of passive flow control is that it cannot be disengaged when not necessary and cannot suit wide range of requirements which may occur during a flight.

Active flow control techniques, on the other hand, require energy or pressurised air from other parts of the engine. Suction, tangential blowing/injection, wall heat transfer, moving wall, vortex generator jets are some of the active flow control techniques. However, in case of suction, blowing/injection, vortex generator jet, mass flow rate is changed (either added or extracted) in the system. For air-intakes, even a slight change in mass flow rate may drastically deteriorate the performance of the downstream components- for example, axial compressor[7].

Received : 04 May 2018, Revised : 28 January 2020
Accepted : 04 March 2020, Online published : 09 March 2020

Therefore, alternative strategies of flow control need to be investigated.

A synthetic jet mechanism consists of a tiny cavity with a moving membrane at the base and an orifice plate at the other end. Throughout an inward motion of the diaphragm, the moving air is sucked into the cavity through the orifice. Once the membrane is moving upward, the fluid within the cavity is ejected creating a ring of vortices at the orifice exit. Continuation of this method at at a particular frequency generates a series of vortices that eventually convects with the flow. Interaction of those vortices with the local physical phenomena (like interaction with boundary layer) produces stream-wise vortical structures that helps in delaying flow separation. Over a single period of oscillation of the diaphragm, there is zero net mass flux (ZNMF) into or out of the cavity, therefore it is also called as ZNMF jets[8]. Since these jets do not contribute any effective mass flow into the system, the chances of performance deterioration of compressor are minimum and are therefore considered as a promising flow control strategy for air-intakes.

The effect of pitch to diameter ratio (*P/D*) on the development of row and array of synthetic jets are studied by Smith & Glezer[8], Guo & Kral[9] and Watson[10-11], *et al.* and found that for a *P/D*> 3, the synthetic jets are unaffected by its neighbouring jets. Nevertheless, all of the above studies were restricted to the interaction of two ZNMF jets. Mathis[12], *et al.* extended the study for more number of circular synthetic jets and found that at ratio *P/D*=6, it corresponded to the greatest capacity of the synthetic jets to promote separation control and flow reattachment. The effect of a row of circular synthetic jets on the flow in a twin air intake has not been explored as yet.

Utturkar[13], *et al.* first used the slotted synthetic jet to investigate its flow characteristics with and without the presence of an external cross-flow in a rectangular flow domain. Later, slotted jets are used in S-shaped diffuser[12], serpentine air-intakes[14] and airfoils[15] for controlling flow separation and associated effects. Oren[16], *et al.* experimentally investigated the characteristics of circular and non-circular synthetic jet configurations and found slot configuration is effective for flow control due to high spreading rate and mixing.

Leschziner & Lardeau[17] also compared the functioning of circular and slotted synthetic jets and discussed the reasons of superiority of slotted jets over the circular jets. Firstly, due to limited lateral spread of circular jet and wide spacing, it failed to energize the massive flow separation adequately. Secondly, the circular jet has less likelihood of making a resonance between the actuation frequency and two-dimensional instability modes within the separated shear layer. Thirdly, the periodic part of the actuated circular jet putrefies quickly at intervals of a couple of jet parameters, that leaves the bulk of the flow separation unaffected by the jet on the far side the jet boundary. Finally, unsteady kinetic energy is considerably raised within the downstream of circular jet injection location, however, there is no proportionate increase of the cross correlation (total shear stress), that is the most responsible for momentum mixing and thence flow separation. This is often considered as a result of the most important periodic perturbation of the circular jet arises within the outer region of the boundary layer.

Chen & Wang[18] computationally investigated the flow control using slotted synthetic jet inside an S-duct diffuser and found that the actuators located at different span-wise positions weaken the secondary flows by delaying the flow separation to get energetic and uniform main flow. However, to the best of the knowledge of the authors, none has used slotted synthetic jets for flow control in twin air-intake ducts. Though the use of array of circular synthetic jet is more common, literature review points that slotted synthetic jet is expected to perform better in comparison to circular synthetic jet, Therefore, the present investigation was planned to test the hypothesis in a twin air intake.

## 2. GEOMETRY

The details of geometry of the twin air-intake used in the study is shown in Fig. 1. The twin air-intake is constructed as per the procedure mentioned in Mathis[19], *et al.* and illustrated in Fig. 1(a). The two arcs of centerline curvature of 20° and a total centreline length of 300 mm till the merging plane C followed by150 mm post-merging length is provided to ensure better mixing of flows before exiting the intake. The air-intake

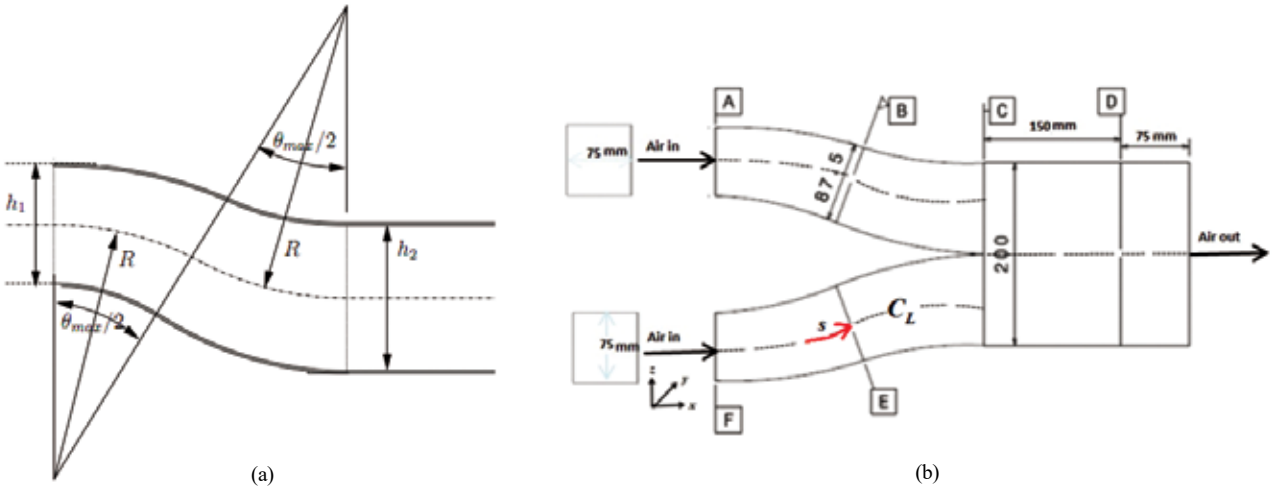


**Figure 1. Schematic diagram of twin air-intake: (a) Centerline curvature of single limb[19] and (b) Mid-plane of twin air-intake.**

has a uniform width of 75 mm throughout its length. The twin air-intake used in this study has rectangular inlet and outlet areas having a ratio of outlet to inlet equal to 1.33. Inlets are shown as planes-A and F, whereas, the outlet plane-D is considered as the AIP (Fig. 1(b)). B and E represent planes of inflexion.

For the present investigation, geometrical parameters for the circular synthetic jet are taken from Mathis[19], *et al.* and geometrical parameters of the slotted synthetic jet are taken from Chen & Wang[18]. Accordingly, the circular synthetic jet actuator (SJA) used in the present investigation has orifice diameter 1.5 mm, orifice height 3 mm, cavity diameter 5 mm, and the cavity height 5 mm. Four such circular synthetic jets in a row are attached to each inner wall of the twin air-intake as shown in Fig. 2(a). Thus, a total of eight circular jets are attached to the two inner walls of the air-intake. These are placed in a spanwise direction along a span of 75 mm. The end jets are located sufficiently far from the side walls to avoid any side wall effect. *P/D* chosen for the circular synthetic jet orifices is 6.

On the other hand, the slotted synthetic jet has a width of 1 mm and a length of 70 mm. Two such slotted jets are attached to the inner walls of the air-intake as shown in Fig. 2(b). Both types of synthetic jets are made an angle of 50° to the mean flow at its exit according to Chen & Wang[18] ensuring smooth entry of the jet into the main flow.

(a) (b)

**Figure 2. Circular and slotted synthetic jets attached to the twin air-intake: (a) Circular jets in a row and (b) Slotted jets in a pair.**

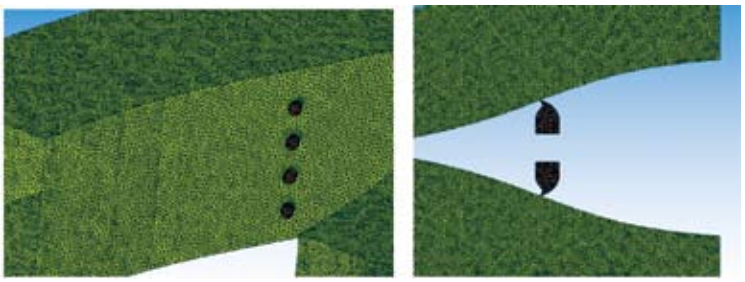

(a) (b)

**Figure 3. Enlarged views of meshed geometry of twin air-intake: (a) Circular jets and (b) Slotted jets.**

## 3. GRID GENERATION

Twin air-intake geometry is meshed using ICEM-CFD unstructured meshing scheme. Quad-dominant and patch-independent meshing method are used which follows robust Octree meshing algorithm Prism/inflation layers are created at the intake boundary to effectively capture the near wall flows leading to lesser numerical diffusion. An enlarged view of mesh geometry of the twin air-intake with circular and slotted synthetic jets are shown in Fig. 3.

## 4. GOVERNING EQUATIONS

The basic governing equations used in this study are shown here.

*Continuity equation:* The equation for conservation of mass for an unsteady, incompressible, three-dimensional flow in terms of vector notation can be written as,

$$\nabla.\vec{V} = 0 \tag{1}$$

*Momentum equation:* Conservation of momentum for an unsteady, incompressible, three-dimensional turbulent flow with no body forces and source terms can be written as,

$$\rho\frac{D\vec{V}}{Dt} = -\nabla p + \mu\left(\nabla^2\vec{V}\right) \tag{2}$$

where $\vec{V}$ is the velocity, ρ is the density and μ is the dynamic viscosity of the fluid.

## 5. TURBULENCE MODEL

Transition shear-stress transport (SST) turbulent model is used to capture the turbulence behavior of the flow in the present simulation. In case of transition SST model, SST $k-\omega$ transport equations are coupled with two more transport equations- one is based on transition onset condition while another is based on flow separation induced transition condition stated in terms momentum thickness Reynolds number. The SST $k-\omega$ turbulence model was developed by Menter[20] to effectively blend the robust and accurate formulation in the near wall region of adverse pressure gradient flows. SST *k*-ω turbulence model was developed to address the shortcoming to capturing near-wall flow phenomena of the *k*-ε turbulence model. The model unites *k*-ω turbulence model and *k*-ε turbulence model in a way that inner zone of boundary layer uses *k*-ω model, but changes into *k*-ε in the outer free shear layer. Transport equations for SST $k-\omega$ model is given as follows,

$$\frac{\partial}{\partial t}(\rho k)+\frac{\partial}{\partial x_j}(\rho k u_i)=\frac{\partial}{\partial x_j}\left(\Gamma_k\frac{\partial k}{\partial x_j}\right)+\tilde{G}_k-Y_k+S_k \tag{3}$$

$$\frac{\partial}{\partial t}(\rho\omega)+\frac{\partial}{\partial x_j}(\rho\omega u_i)=\frac{\partial}{\partial x_j}\left(\Gamma_\omega\frac{\partial \omega}{\partial x_j}\right)+G_\omega-Y_\omega+D_\omega+S_\omega \tag{4}$$

where $G_k$ and $G_\omega$ represent a generation of turbulent kinetic energy ($k$) and specific dissipation rate ($\omega$) respectively. $\Gamma_\kappa$ and $\Gamma_\omega$ represents effective diffusivity of $k$ and ω respectively. $Y_\kappa$ and $Y_\omega$ are dissipation due to turbulence. $D_\omega$ represents cross-diffusion term while $S_k$ and $S_\omega$ represent user-defined source terms.

Similarly, transport equation for intermittency (γ) and for transition momentum thickness Reynolds number ($\tilde{\mathrm{Re}}_{\theta t}$) is given by,

$$\frac{\partial(\rho\gamma)}{\partial t}+\frac{\partial(\rho U_j\gamma)}{\partial x_j}=P_{\gamma1}-E_{\gamma1}+P_{\gamma2}-E_{\gamma2}+\frac{\partial}{\partial x_j}\left[\left(\mu+\frac{\mu_t}{\sigma_\gamma}\right)\frac{\partial\gamma}{\partial x_j}\right] \tag{5}$$

$$\frac{\partial(\rho\,\tilde{\mathrm{Re}}_{\theta t})}{\partial t}+\frac{\partial(\rho U_j\,\tilde{\mathrm{Re}}_{\theta t})}{\partial x_j}=P_{\theta t}+\frac{\partial}{\partial x_j}\left[\sigma_{\theta t}(\mu+\mu_t)\frac{\partial\tilde{\mathrm{Re}}_{\theta t}}{\partial x_j}\right] \tag{6}$$

where $P_\gamma$ and $E_\gamma$ are source terms which depend on empirical

correlations. μ and $\mu_t$ are dynamic and turbulent viscosities respectively.

## 6. BOUNDARY CONDITIONS

Inlet boundaries are defined as velocity inlets and outlet boundaries as pressure outlet. An experimental velocity profile[21] corresponding to mass-averaged velocity of 20m/s (Re = $1.03\times10^5$) is specified at the inlet of the twin air-intakes. Reynolds number independency for similar air-intake was earlier performed by Singh[22], *et al.* revealing that the performance characteristics are nearly independent of the Reynolds numbers. Zero gauge pressure is set at the outlet of the air-intake. No slip and adiabatic conditions are provided at the walls. The mid-longitudinal plane is considered as the symmetrical plane and the CFD simulation is done only on the half portion of the total flow domain due to symmetry with respect to geometry and flow in the air-intake.

The most crucial part of the CFD simulation of the synthetic jet is the modelling of the vibrating diaphragm. There are three techniques used to model the vibrating diaphragm of SJA[8]. In the present study, moving boundary condition is not applied. Rather a periodic velocity-inlet boundary condition is applied at the neutral position which nearly approaches to moving membrane boundary condition. The periodic velocity inlet boundary condition is given by,

$$U = U_{amp}\sin(2\pi ft) \quad (7)$$

where $U_{amp}$ = velocity amplitude, $f$ = frequency of oscillation. $t$ = time period. A user defined function (UDF) is written for oscillating velocity and extracted at diaphragm of the circular and slotted synthetic jets.

## 7. SOLUTION METHODOLOGY

The governing equations are discretised using the finite volume technique (FVM) on an unstructured, collocated and staggered grid arrangement. Second-order, upwind spatial discretisation scheme and implicit transient formulation is employed for all flow variables. For pressure and velocity coupling, a semi-implicit method for pressure linked equations (SIMPLE) based scheme developed by Patankar[23] is employed. Unsteady, three-dimensional CFD simulation is carried out using CFD solver Ansys-Fluent[24]. The convergence criteria are set as $10^{-5}$ for all solutions.

## 8. GRID INDEPENDENCY STUDY

Since the size of the grid elements has a great impact on CFD solution, grid independency study is performed at different grid sizes for all the three cases. For example, grid independency study of uncontrolled air-intake in terms of static pressure recovery coefficient ($C_{PR}$) is shown in Fig. 4. Roache[25] introduced grid convergence index (GCI) method, which helps in finding discretisation error for the $C_{PR}$ and thus represents a robust quantification of grid independency. In Table 1, low value of GCI indicates grid independency. Accordingly, $C_{PR}$ value is found grid independent at around $9\times10^5$ grid elements.

The time-step refinement study is carried out for the grid elements of about $9\times10^5$ at 200 Hz frequency using different time steps of 1/50 to 1/600 a cycle as shown in Table 2. Based on values of $C_{PR}$ obtained for each case, time step of 1/500 a cycle is chosen to resolve the fluid flow characteristics in time domain.

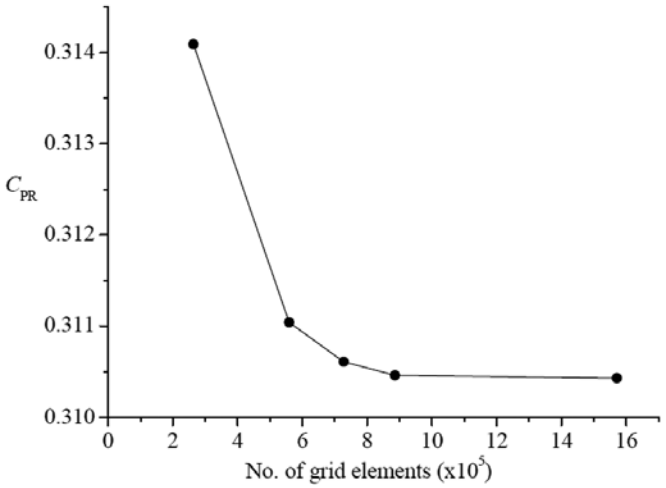


**Figure 4. Grid independency test for uncontrolled air-intake.**

**Table 1. Grid convergence index (GCI) for uncontrolled air-intake**

| No. of mesh elements | $C_{PR}$ | Successive change in $C_{PR}$(%) | GCI (%) |
|---|---|---|---|
| 264000 | 0.31409 | --- | --- |
| 559271 | 0.31104 | −0.97% | 1.413% |
| 727873 | 0.31061 | −0.14% | 2.328% |
| 886169 | 0.31046 | −0.05% | 0.342% |
| 1571640 | 0.31043 | −0.01% | 0.001% |

**Table 2. Time step independency study for controlled SJA**

| Time step for a cycle | Time period | $C_{PR}$ |
|---|---|---|
| 1/50 | $1\times10^{-4}$ | 0.682224 |
| 1/100 | $5\times10^{-5}$ | 0.687275 |
| 1/250 | $2\times10^{-5}$ | 0.694176 |
| 1/500 | $1\times10^{-5}$ | 0.694373 |
| 1/600 | $8.33\times10^{-6}$ | 0.694338 |

## 9. VALIDATION OF CFD MODEL

The computational results for both uncontrolled and controlled cases are validated against the results reported in the literature. The following sub-sections present the validation of CFD results.

### 9.1 Validation of Uncontrolled Twin Air-intake

The computational results of uncontrolled twin air-intake are validated with the experimental results reported by Paul[21]. The pressure and velocity measurement in the twin air-intake was carried out using a five-hole pressure probe connected with digital pressure sensors. Experimental turbulent velocity profile thus measured, was imposed at the inlet of the computational domain. The validation of static pressure recovery coefficient ($C_{PR}$) along the streamline length ($s$) normalised by centreline length ($C_L$) of air-intake is presented in Fig. 5. The static pressure is seen gradually increasing due to are diffusion,

attains a maximum value at the merging plane ($s/C_L$ = 0.667), and then decreases due to constant-area duct connected in the post-merger section. Both the experimental and computational results exhibits the similar trends, while showing maximum variation around 10 per cent, which is considered reasonable and within acceptable limit.

### 9.2 Validation of Controlled Twin Air-intake

For the validation of twin air-intake with synthetic jets, experimental results reported by Mathis[19], *et al*. for S-shaped air-intake (refer Fig. 1a) is used. The experiments were conducted at a centreline velocity ($U_c$) of 12.4 m/s, corresponding to a Reynolds number at the S-shaped leading edge of about Re ($U_c h_c/\nu = 4.1\times10^4$), where $h_c = 0.h_1$, $h_1$ being the height of the inlet section of the S-shaped duct. The turbulence intensity of the flow at the S-duct inlet was found to be around 1.35 per cent. For unsteady flows, experimental and present computational and results are furnished in Table 3.

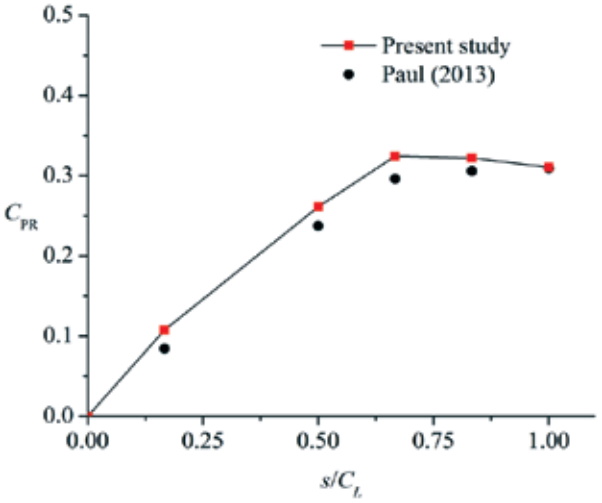


**Figure 5. Validation of static pressure coefficient ($C_{PR}$) in uncontrolled air-intake.**

Flow separation point and the boundary layer thickness during suction and blowing are calculated. It is noted that the boundary layer thickness mentioned in Table 3 is calculated at a point just before the flow separation begins. The computational results varied 9-15 % from the experimental results, which are in acceptable agreement. The variation is due to the limitation of the RANS turbulence model used in predicting the near wall flow features as compared to large-eddy simulation.

## 10. RESULTS AND DISCUSSION

This section contains results and discussion of computational simulations for both uncontrolled and controlled cases of twin air-intake with circular and slotted synthetic jets.

### 10.1 Velocity Contours

A flow separation zone is generated from the inner walls of the uncontrolled twin air-intake, which subsequently merged at plane-C and then convects further downstream (Fig. 6(a)). Along the streamline direction, flow separation is started at $s/C_L$= 0.208. However, with the use of circular or slotted synthetic jets attached just upstream of the location of flow separation points at the inner walls of the air-intake, the flow separation zone is reduced to a great extent (Figs. 6(b) and 6(c)). For circular jet, flow separation point is shifted downstream ($s/C_L$= 0.524), while in case of slotted jet, the separation point is moved further downstream ($s/C_L$= 0.610) indicating the efficacy of slotted synthetic jets over the circular one.

### 10.2 Development of Vortices

Figures 7 and 8 show the iso-surface of vortices generated at different phases of circular and slotted synthetic jets respectively. During blowing phase (Fig. 7(a)) of circular synthetic jets (at $t$=$T$/4), main core flow is energised due to the ejection of high momentum air jet through orifice. Vortices however, do not have spanwise elongation in case of circular synthetic jets as shown in Fig. 7(a). At $t$ = $T$/2,vortices are separated from

**Table 3. Comparison of flow separation point**

| | Uncontrolled duct | | Controlled duct | |
|---|---|---|---|---|
| | Separation point ($x/h_1$) | Boundary layer thickness ($\delta/h_1$) | Boundary layer thickness ($\delta/h_1$) | |
| | | | Maximum blowing | Maximum suction |
| Experimental results[19] | 0.0735 | 0.1668 | 0.1616 | 0.1578 |
| Present computational results | 0.0805 | 0.1411 | 0.1403 | 0.1308 |

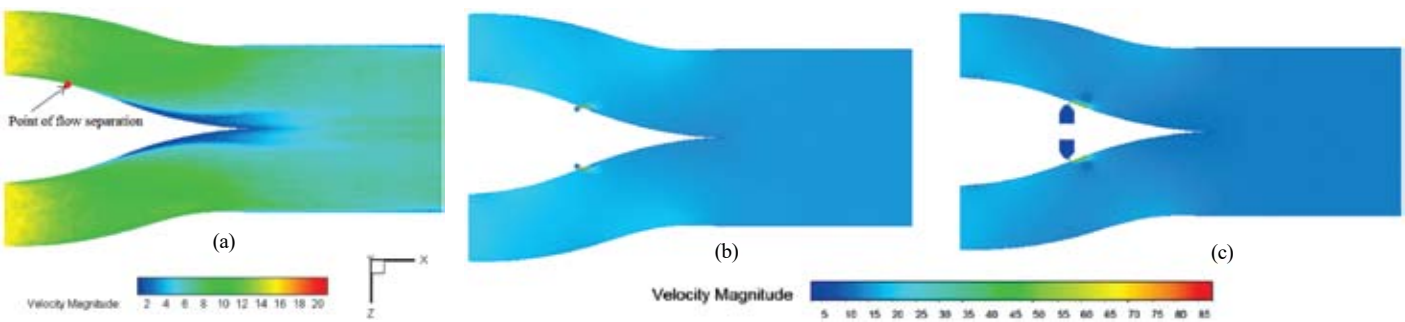


**Figure 6. Velocity contours at mid-plane of the twin air-intake (a) uncontrolled case, (b) with circular jets at $t$=$T$/4, and (c) with slotted jets at $t$=$T$/4.**

the orifice and increases in size while moving downstream (Fig. 7(b)). During suction phase, synthetic jets suck low momentum air near the orifice into the jet cavity without interfering the vortices created during ejection (Fig. 7(c)). At $t$=3$T$/4, maximum suction exists and the involvement of primary vortex ring is over (Fig. 7(d)).

When slotted synthetic jets are employed in twin air-intake, a set of primary vortices is created close to the exit of slotted jet at the onset of blowing phase (Fig. 8(a)). The vortices are almost rectangular in shape, extended in the streamwise direction owing to geometrical features of the slot. At $t$=$T$/2, the vortices move downstream and a secondary instability occurs in the spanwise direction, resulting in the break-up of the primary vortex structures owing to three-dimensional vortex stretching[26]. This secondary ring is strongly influenced by the primary ring as it accelerates soon after being shed. The size of this secondary ring is much smaller compared to the primary ring, as the ring cannot grow in size greatly due to the accelerating effect of the primary ring. It is noted that the following breakdown of the secondary vortices is accountable for the transition to turbulence as shown at $t$ = $T$/2 in Fig. 8(b). As the suction phase of the circle starts (Fig. 8(c), the vortices are strongly influenced by ambient fluid into the slot. At $t$ =$T$, The vortex pair inside the cavity start to increase while it descends and engulfs the cavity before the next cycle is begun.

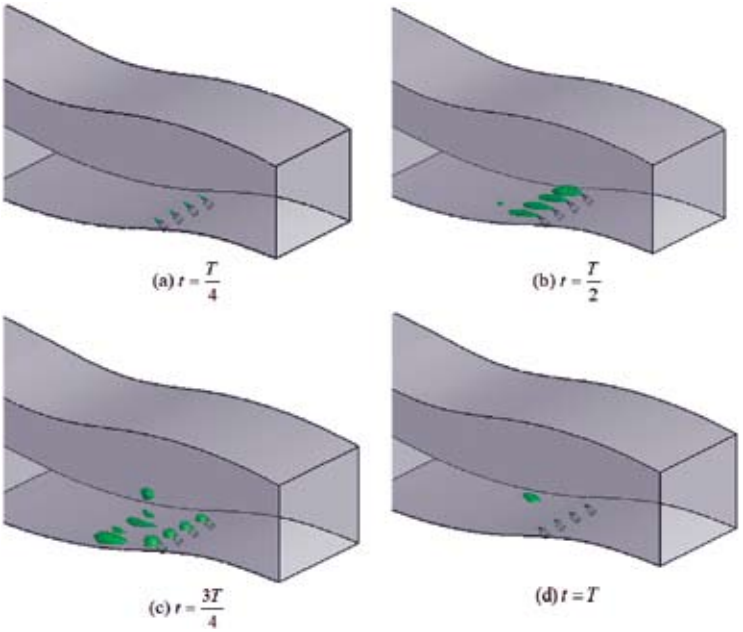


**Figure 7. (a-d): Development of vortices through circular synthetic jets at different time periods.**

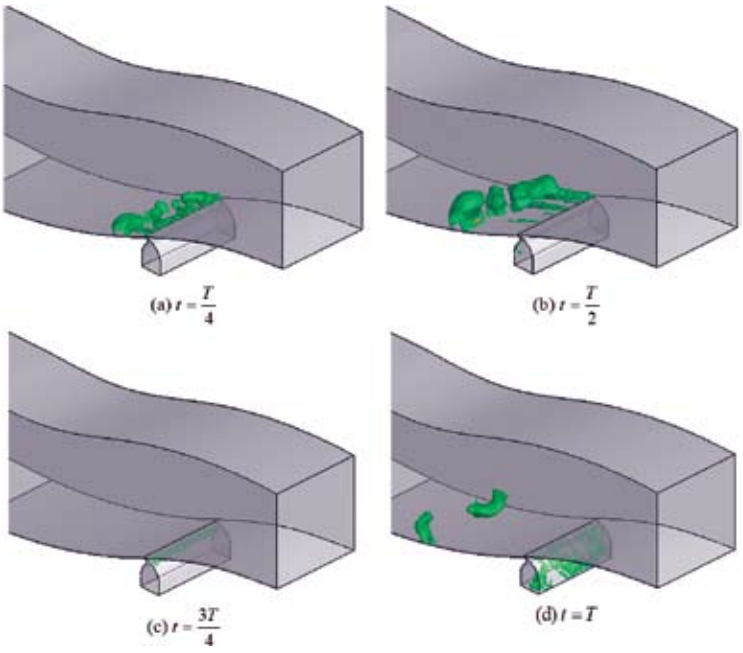


**Figure 8. (a-d): Development of vortices through slotted synthetic jets at different time periods.**

The slotted jets have a greater control authority as compared to circular jets as seen by comparing Figs. 7(d) and 8(d). This is due to the spanwise distribution of the vortices and the mass and vorticity ejected leading to better mixing as compared to the circular jets. During blowing phase, vorticity strength for the slotted jets is computed as 203 $s^{-1}$ at AIP, while for circular jets, its value is 198$s^{-1}$. Hence, slotted synthetic jets offers more energised momentum as compared to an array of circular jets.

For the present study, the frequency at which both the slotted and circular synthetic jets operate is same ($f$=200 Hz). The total energy supplied by the slotted and circular jets into the air-intake per second are calculated as 0.05 J and 0.1 J respectively. The energy loss is less with the use of slotted jets (4.88 J) as compared to the circular jets (6.92 J). The jet configuration which can efficiently control the flow separation and improve other aerodynamic performance parameters with the lowest input of energy is considered best (Mathis[12], *et al*.). Hence, in the present study, slotted synthetic jet configuration is considered best option of flow control for the twin air-intake. These reasons are collectively responsible to explain why slotted jets outperforms circular jets to control flow separation and thereby increase aerodynamic performance of the twin air-intake. The subsequent sub-sections discuss the global aerodynamic performance parameters of the twin air-intake duct, which are evaluated at the aerodynamic inlet plane.

### 10.3 Static Pressure Recovery Coefficient

Static pressure recovery coefficient defines the effectiveness of air-intake to recover the static pressure at the outlet (AIP) and it is defined as the ratio of the increase in average static pressure with reference to the inlet to average dynamic pressure at the inlet. Mathematically,

$$C_{PR} = \frac{p_s - p_{si}}{\frac{1}{2}\rho U_{avi}^2} \tag{8}$$

where $P_s$ is the mass-averaged static pressure at any plane and $P_{si}$ is the mass-averaged static pressure at the inlet.

Flow separation and strong secondary flow gradient result in decrease in $C_{PR}$ at the exit of air-intake. It is observed

from Fig. 9 that $C_{PR}$ is increased with the use of synthetic jets employed in twin air-intake. When circular synthetic jets are used, a marginal increase in $C_{PR}$ is noticed. However, with the use of slotted synthetic jets, 15.14 % of increment in $C_{PR}$ is observed at $s/C_L$= 0.8 from the inlet of air-intake duct.

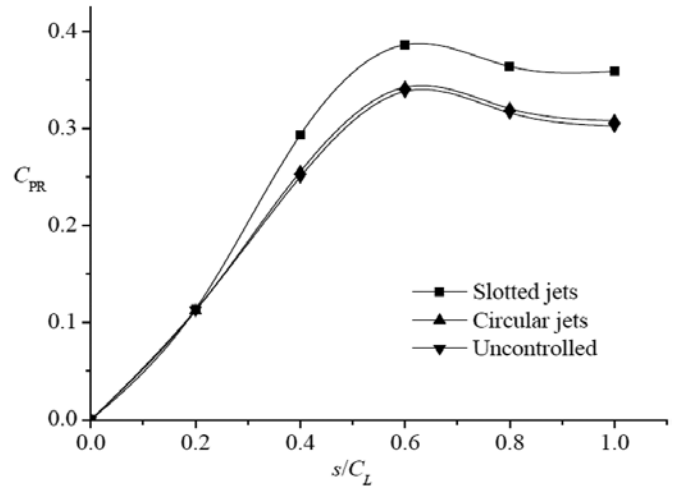


**Figure 9. Variation of $C_{PR}$ along the length of air-intake for controlled and uncontrolled cases.**

### 10.4 Total Pressure Loss Coefficient ($C_{TL}$)

The total pressure that refers to the whole energy contained within the fluid. The low energy fluid within the boundary layer is extremely liable to adverse pressure gradients resulting in flow separation. Because of viscous diffusion and associated with the growth of boundary layer, flow separation occurs and a rise in the secondary flow causes loss in total pressure at the downstream of twin air-intake. Reduction of total pressure losses is hence essential.

The expression for total pressure loss coefficient, $C_{TL}$ is given as the ratio of total pressure loss with respect to the inlet to the average dynamic pressure at the inlet.

$$C_{TL} = \frac{(P_{Ti} - P_T)}{\frac{1}{2}\rho U_{avi}} \tag{9}$$

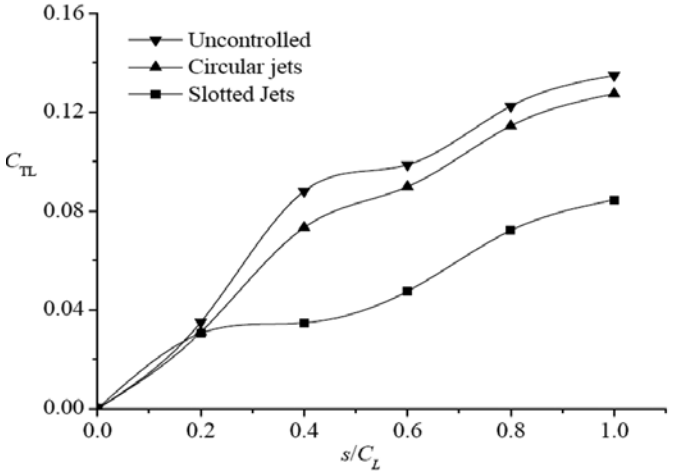


**Figure 10. Variation $C_{TL}$ along the length of air-intake for controlled and uncontrolled cases.**

where $P_{Ti}$ is the mass-averaged total pressure at inlet and $P_T$ is the mass-averaged total pressure at any plane.

In the present investigation, the decrement of $C_{TL}$ is observed in Fig. 10 with the use of both types of slotted jets. In case of circular synthetic jets, $C_{TL}$ is decreased by 6.57%, while the same for slotted synthetic jets is a whopping 41.11% as compared to uncontrolled baseline flow in air-intake.

### 10.5 Distortion coefficient

The total pressure distortion at the engine face is one in all the parameters that contribute to the intake losses. The distortion is either steady or unsteady and could be a vital reason for premature engine surge named as 'buzz'. Engine surge is caused by stall of the rotating components like blades and can create reverse flow leading to a sharp reduction in engine thrust[27]. This kind of distortion (surge or buzz) cause a variety of undesirable effects as well as uneven pressure loading of the rotating components and can result in reverse flow resulting in a drastic reduction in the engine thrust[27]. This type of distortion (surge or buzz) can cause a range of undesirable effects including asymmetric pressure loading of the compressor blades, which in turn, threaten the engine with flameout.

The main distortion descriptor used for present calculation is $DC_{60}$. The parameter tries to relate the region of maximum losses to the averaged losses over the entire face. The engine face or (AIP) is virtually divided into numerous overlapping 60° wedges, the total pressure over which is averaged. The $P_{60}$ in Eqn. (10) is the minimum of the total averaged pressure of all the wedges, while $q_{avg}$ is the dynamic pressure at the AIP. Mathematically,

$$DC_{60} = \frac{P_T - P_{60}}{q_{avg}} \tag{10}$$

In case of circular synthetic jets, a decrement of 11.11% in distortion is computed at the exit of the air-intake. However, in case of slotted synthetic jets, the reduction in $DC_{60}$ is by 38.50% as compared to the uncontrolled air-intake.

### 10.6 Secondary Flow Non-uniformity

Secondary velocity ($V_{yz}$) present in the flow field increases adverse pressure gradient near the wall of the diffuser, causes enhancement of flow separation. The secondary velocity non-uniformity index ($S_{io}$) at duct outlet (AIP) can be defined as the average of the sum of secondary velocities ($V_{yz}$ in $y$-$z$ plane), non-dimensionalised by the average velocity at the inlet. Mathematically,

$$S_{io} = \sum\left(\frac{V_{yz}}{(n * U_{avi})}\right) \tag{11}$$

where $n$ is the number of computational data points considered at the AIP.

Figure 11(a) shows two prominent vortices on upper and lower half of the air-intake at the AIP depicting the non-uniformity in the flow at its engine face. However, with the introduction of synthetic jets, the flow pattern at the AIP has changed into more uniform. In the present investigation, it is found that secondary velocity is decreased after employing

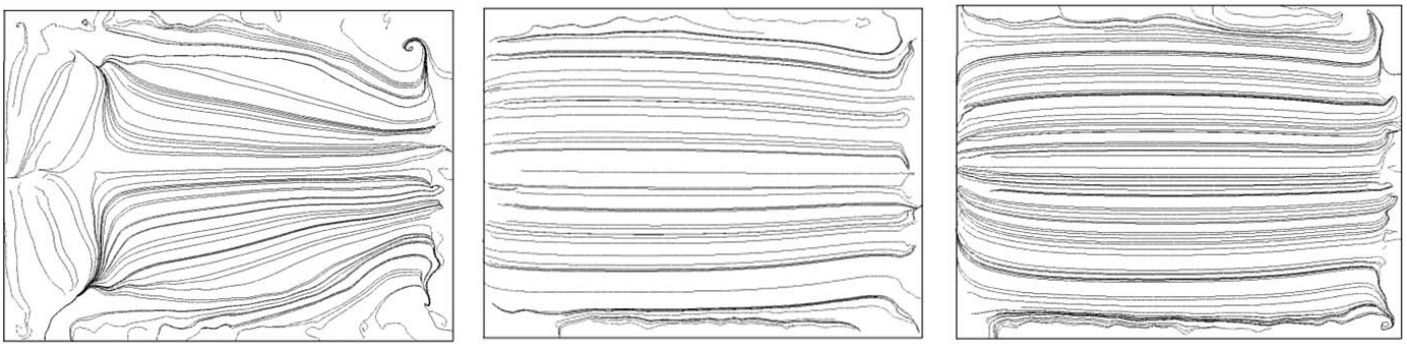


**Figure 11. Streamline velocity plot at the AIP of air-intake for controlled and uncontrolled cases (a) Uncontrolled ($S_{io}$= 0.601), (b) With circular jets ($S_{io}$= 0.431), and (c) With slotted jets ($S_{io}$= 0.387).**

synthetic jets, so is the secondary non-uniformity. In case of circular and slotted synthetic jets, secondary flow non-uniformity is decreased by 28 per cent and 35 per cent, respectively with respect to the uncontrolled case.

## 11. CONCLUSIONS

Computational analysis of flow field in a twin air-intake with or without flow control techniques are investigated in the present study. The major findings are listed below.

- Flow separation in twin air-intake duct is eliminated with the use of both circular and slotted synthetic jets. Vorticity dynamics reveals that lateral spread of the circular jets is limited as compared to the slotted jet.
- A maximum increment of 15.14 % in static pressure recovery ($C_{PR}$) is observed in case of slotted synthetic jets as compared to uncontrolled flow and also 41.11% of $C_{TL}$ decrement is found in case of slotted synthetic jets.
- The main distortion descriptor used for present calculation is distortion coefficient ($DC_{60}$) and it is found that 38.5 % of decrement in $DC_{60}$ in case of slotted synthetic jets.
- It is observed that secondary velocity decreases so is the secondary flow non-uniformity ($S_{io}$) using both flow control techniques. $S_{io}$ is computed minimum (35% with respect to the uncontrolled case) in case of slotted synthetic jets.
- The results effectively demonstrate the efficacy of slotted synthetic jets over a row of circular synthetic jets for controlling flow in twin air-intake.

## REFERENCES


1. Mayer, D.W.; Anderson, B.H. & Johnson, T. A. 3D subsonic diffuser design and analysis, *Am. Inst. Aeronautics Astronautics,* AIAA 98-3418, 1998. doi: 10.2514/6.1998-3418
2. MacMartin, D.G.; Verma, A.; Murray, R.M. & Paduano, J. D. Active control of integrated inlet/compression systems. *In* Proceedings of ASME FEDSM 2001: ASME Fluids Engineering Division Summer Meeting New Orleans, Louisiana, 2001.
3. Gad-el-Hak, M. Flow control: Passive, active and reactive flow management. Cambridge University Press, 2000.
4. Abdellatif, O.E. Experimental study of turbulent flow characteristics inside a rectangular S-shaped diffusing duct. *Am. Inst. Aeronautics Astronautics, AIAA* 2006-1501, 2006, doi:10.2514/6.2006-1501
5. Paul, A.R.; Joshi, S.; Jindal, A.; Maurya, S.P. & Jain, A. Experimental studies of active and passive flow control techniques applied in a twin air-intake. *Sci. World J.*, 2013, 1-8. doi: 10.1155/2013/523759
6. Keerthi, M.C. & Kushari, A. Effectiveness of vortex generator jets and wall suction on separated flows in serpentine-duct diffuser. *Aerospace Sci. Technol.*, 2014, **34**(1), 12-19. doi:10.1016/j.ast.2014.01.013.
7. Seddon, J.M. & Goldsmith, E.L. Intake Aerodynamics, AIAA Education series, Wiley Blackwell, 1998.
8. Smith, B.L. & Glezer, A. The formation and evolution of synthetic jets. *Physics Fluids*, 1998, **10**(9), 2281-2297. doi: 10.1063/1.869828
9. Guo, D. & Kral, L.D. Numerical simulation of the interaction of adjacent synthetic jet actuators, AIAA paper 2000-2565, 2000. doi: 10.1007/978-3-642-59334-5_114.
10. Watson, M.; Jaworski A. J. & Wood N. J. Contribution to the understanding of flow interactions between multiple synthetic jets, *AIAA J.*, 2003, **41**(4), 747–749. doi: 10.2514/2.2008
11. Watson M.; Jaworski A. J. & Wood N. J. A study of synthetic jets from rectangular and dual-circular orifices. *Aeronautical Journal*, 2003, **107**(3), 427–434. doi: 10.1017/S000192400001335X.
12. Mathis, R.; Duke, D.; Kitsios, V. & Soria, J. Flow control in S-shaped air-intake using zero-net-mass-flow. *In* 16th Australasian Fluid Mechanics Conference, Australia, 2007.
13. Utturkar, Y.; Mittal, R.; Rampunggoon, P. & Cattafesta, L. Sensitivity of synthetic jets to the design of the jet cavity. *In* 40th AIAA Aerospace Sciences and Exhibit 0124, 2002. doi: 10.2514/6.2002-124.
14. Kumar, A. Flow control optimization in a jet engine serpentine inlet duct, Texas A&M University, 2007.

(Master thesis).
15. Guoqing, Z. & Qijun, Z. Parametric analyses for synthetic jet control on separation and stall over rotor airfoil. *Chinese J. Aeronautics*, 2014, **27**(5), 1051-1061. doi: 10.1016/j.cja.2014.03.023.
16. Oren, L.; Gutmark, E.; Muragappan, S. & Khosla, S. Flow characteristics of non circular synthetic jets. *In* 47th AIAA Aerospace Sciences Meeting Including the New Horizons Forum and Aerospace Exposition, 2009, Orlando, Florida, 2009, 1309. doi: 10.2514/6.2009-1309.
17. Leschziner, M.A. & Lardeau, S. Simulation of slot and circular synthetic jets in the context of boundary-layer separation control. *Philosophical Trans. Royal Society- A*, 2011,369, 1495–1512. doi: 10.1098/rsta.2010.0363
18. Chen, Z.J. & Wang, J.J. Numerical investigation on synthetic jet flow control inside an S-inlet duct. *Sci. China Technol. Sci.*, 2012, **55**(9), 2578–2584. doi: 10.1007/s11431-012-4970-y.
19. Mathis, R.; Duke, D.; Kitsios, V. & Soria, J. Use of zero-net-mass-flow for separation control in diffusing S-duct. *Experimental Thermal Fluid Science*, 2008, **33**, 169–172. doi: 10.1016/j.expthermflusci.2008.07.005
20. Menter, F. R. Two-equation eddy-viscosity turbulence models for engineering applications. *AIAA Journal,* 1994, **32**(8), 1598–1605. doi: 10.2514/3.12149
21. Paul, A.R. Aerodynamic studies of turbulent flow in twin air-intakes, Department of Applied Mechanics, Motilal Nehru National Institute of Technology Allahabad, India, 2013, Ph.D. Thesis.
22. Singh, R.K.; Singh, S.N. & Seshadri, V. Performance and flow characteristics of double-offset Y-shape aircraft intake duct. *J. Aircraft*, 2008, **45**(2), 1230-1243. doi: 10.2514/1.34137
23. Patankar, S.V. Numerical heat transfer and fluid flow. Taylor and Francis Publication, London, 1980.
24. Ansys-Fluent 15.1, User's Guide, Ansys Inc., Canonsburg, PA 15317,2015.
25. Roache, P.J., Fundamentals of Verification and Validation, Hermosa Publishers: New Mexico, USA, 2009.
26. Palumbo, A.; Chiatto, M. &de Luca, L. Measurements versus numerical simulations for slotted synthetic jet actuator. *Actuators* 2018, **59**(7), 1-15. doi:10.3390/act7030059
27. Oates, G.C. The aerodynamics of gas turbines and rocket propulsion, AIAA Education Series, NY, 1984. doi: 10.2514/5.9781600861345.0000.0000

## ACKNOWLEDGEMENT

The research is extensively supported by the Science and Engineering Research Board, Department of Science and Technology (SERB), Government of India through SERB Start-up Grant for Young Scientists awarded to Dr Akshoy Ranjan Paul, Assistant Professor, Department of Applied Mechanics, MNNIT Allahabad, India vide sanction order no. SB/FTP/ETA-24/2013 dated 16/08/2013.

## CONTRIBUTORS

**Mr Krishnakumar Rajnath Yadav** completed BTech (Mechanical Engineering) from Mumbai and MTech (Mechanical Engineering) from NIT Patna. He specialises in fluid mechanics and refrigeration engineering and has published a few research papers in aerodynamics and thermo-fluids engineering in refereed journals and international conferences. He is currently pursuing PhD from MNNIT Allahabad.
He carried out the CFD analysis and also wrote the paper.

**Dr Akshoy Ranjan Paul** has received BTech and MTech in Mechanical Engineering, while he did PhD from MNNIT Allahabad. He is an Associate Professor at the Department of Applied Mechanics, MNNIT Allahabad, India and is involved in teaching and research for 18 years. He has published over 125 research papers on experimental fluid dynamics, flow control, CFD and green energy and wrote four textbooks. He is the reviewers of many journals and conducted various conferences, workshops, short-term courses on a plethora of topics. He has handled four externally funded research projects so far.
He is the principal investigator under which the research work reported in the paper was carried out.

**Mr Nithin Hegde** did his bachelor's in Aeronautical Engineering and later completed MTech (Fluids Engineering) from MNNIT Allahabad. He specialises in computational modelling of internal flows and published some research papers in conferences to his credit. Presently he is working in Cummins India Ltd., Pune.
He worked on CAD and flow modelling of the problem discussed in the paper.

**Dr Anuj Jain** has completed his PhD in Chemical Engineering from IIT Roorkee. Currently he is a Professor at the Department of Applied Mechanics, MNNIT Allahabad, India. He has over 30 years of research experience in thermo-fluid flows, multiphase flows and bio-fluid dynamics and has published over 150 research articles in peer-reviewed journals and reputed conferences in India and abroad. He served at various academic and administrative positions during his career, authored two textbooks, supervised numerous MTech and PhD theses and handled three government sponsored research projects.
Contribution in the current study, he acted as an advisor to the research work reported in the paper.